

GEOID UNDULATIONS CHART OF THE SAN LUIS RANGE (ARGENTINA). GEOPHYSICAL APPLICATION

Laura L. CORNAGLIA & Antonio INTROCASO



**Boletín
del Instituto de
Fisiografía y Geología**

Cornaglia L.L. & Introcaso A., 2008. Geoid undulations chart of the San Luis range (Argentina). Geophysical application. *Boletín del Instituto de Fisiografía y Geología* 78(1-2): 13-22. Rosario, 02-12-2008. ISSN 1666-115X.

Abstract.- In this work we show that it is possible to define the isostatic state of a geological structure using a geoid undulations chart. We have built: (1) a detailed geoid undulations chart of the San Luis range area using (a) the global geopotential model EIGEN CG03C for long wavelength free-air gravity anomalies and geoid undulations, and (b) observed residual free-air gravity anomalies and the equivalent sources method for short wavelength geoid undulations, and (2) a theoretical undulations chart of San Luis range area, involving effects from an isostatically compensated model. By comparing charts (1) and (2) we have found agreement between them, thus indicating the San Luis range is rather well isostatically balanced.

Key-words: Geological structure; Geoid; Isostasy.

Resumen.- Carta de ondulaciones del geoide de la Sierra de San Luis (Argentina). Aplicación geofísica. Nuestro propósito es demostrar que desde una carta de ondulaciones del geoide de buena resolución es posible inferir las características corticales de una estructura geológica. Para ello construimos: (1) una carta de ondulaciones del geoide sobre la sierra de San Luis con adecuado detalle empleando (a) anomalías de aire libre y ondulaciones del geoide de largas longitudes de onda provenientes del modelo global geopotencial EIGEN CG03C y (b) anomalías de aire libre residuales observadas y el método de fuentes equivalentes para calcular las ondulaciones del geoide de cortas longitudes de onda, y (2) una carta de ondulaciones del geoide que contiene los efectos isostáticos de un modelo perfectamente compensado. Comparando ambas cartas (1) y (2) encontramos una muy aceptable coincidencia entre ambas, indicando un buen balance isostático para la sierra de San Luis.

Palabras clave: Estructura geológica; Geoide; Isostasia.

Laura L.Cornaglia: *Instituto Geofísico Sismológico Volponi (UNSJ), Meglioli 1160 (S), 5400 San Juan, Argentina, Grupo de Geofísica, IFIR (CONICET-UNR), Pellegrini 250, 2000 Rosario, Argentina.*

Antonio Introcaso: *Facultad de Ciencias Exactas, Ingeniería y Agrimensura (UNR), Grupo de Geofísica, IFIR (CONICET-UNR), Pellegrini 250, 2000 Rosario, Argentina.*

Received: 01/08/2008; accepted: 15/11/2008.

INTRODUCTION

The San Luis range is located NE of the homonymous Province, west-central Argentina. The range boundaries are: 32°00'– 33°30' S and 65°00'– 66°30' W. The range extends over 23000 km² along an imaginary axis 150 km long and NE strike. The range is 80 km wide. Altitudes are less than 2000 m. Three sedimentary basins are located around the San Luis range: Las Salinas in the Northwest, Beazley in the South, Mercedes in the Southeast and Conlara Valley apart from the San Luis range of Comechingones range (Fig. 1).

Cornaglia & Introcaso (2004), working on a profile, have preliminarily pointed out a crustal thickness excess in the area; Crovetto & Introcaso (2004) have proposed short wavelength isostatic geoid indicators to make a preliminary isostatic analysis of the San Luis range, concluding that geoid undulations allow validating classic gravimetry; Introcaso & Crovetto (2005) have presented different methods for building a geoid chart, in particular a chart for the San Luis range. All previous works on the San Luis range have presented preliminary conclusions because of the lack of consistent geoid undulations charts.

In this work we present a high resolution geoid undulations chart built using an equivalent sources method and observed free-air gravity anomalies (Fig. 2), practically Faye anomalies in view of the maturity of the topography. We have first obtained long wavelength geoid undulations (N_{LWL}) using adequate cuts in the spherical harmonic expansions. We have used the global geopotential models EGM96 (Lemoine et al. 1998) and EIGEN GL03C (Förste et al. 2005). Then, from residual free-air gravity anomalies and equivalent sources

methods, we have obtained short wavelength geoid undulations N_{SWL} . Total geoid undulations are: $N_T = N_{LWL} + N_{SWL}$. This expression was adjusted in eleven geoid height stations $N = h - H$ (see Fig. 3). Finally, from San Luis range topographic altitudes, we have built an isostatically balanced model defined using T_N (standard crustal thickness): 33 km and R (crustal root below T_N) = $6.675 H_T$, being H_T the topographic altitude. From direct calculation and using right and homogeneous parallelepipeds we have obtained theoretical residual free-air gravity anomalies corresponding to the isostatically compensated model. Then, using the equivalent sources method, we have obtained the disturbing potential T and the isostatic geoid undulations N_{ISWL} . Total isostatic geoid undulations are $N_{IT} = N_{LWL} + N_{ISWL}$. By comparing N_T and N_{IT} we have found that the San Luis range is isostatically rather well balanced.

BRIEF DESCRIPTION OF THE SAN LUIS RANGE

Jordan & Allmendinger (1986) have pointed out that the Pampeanas Ranges geological province of Argentina is a region of large mountains. It is located on the western side of the thin skinned thrust belt of the Andean Mountains, coincident with a region where the subducted Nazca plate is sub-horizontal. Mountain ranges have been uplifted by reverse faulting and local folding. There are evidences of compressional earthquakes. The nearest shortening is estimated to be about 2%. Many of the faults are listric in the subsurface and flatten at mid to lower crustal depths. In opinion of Sato et al. (2003), the

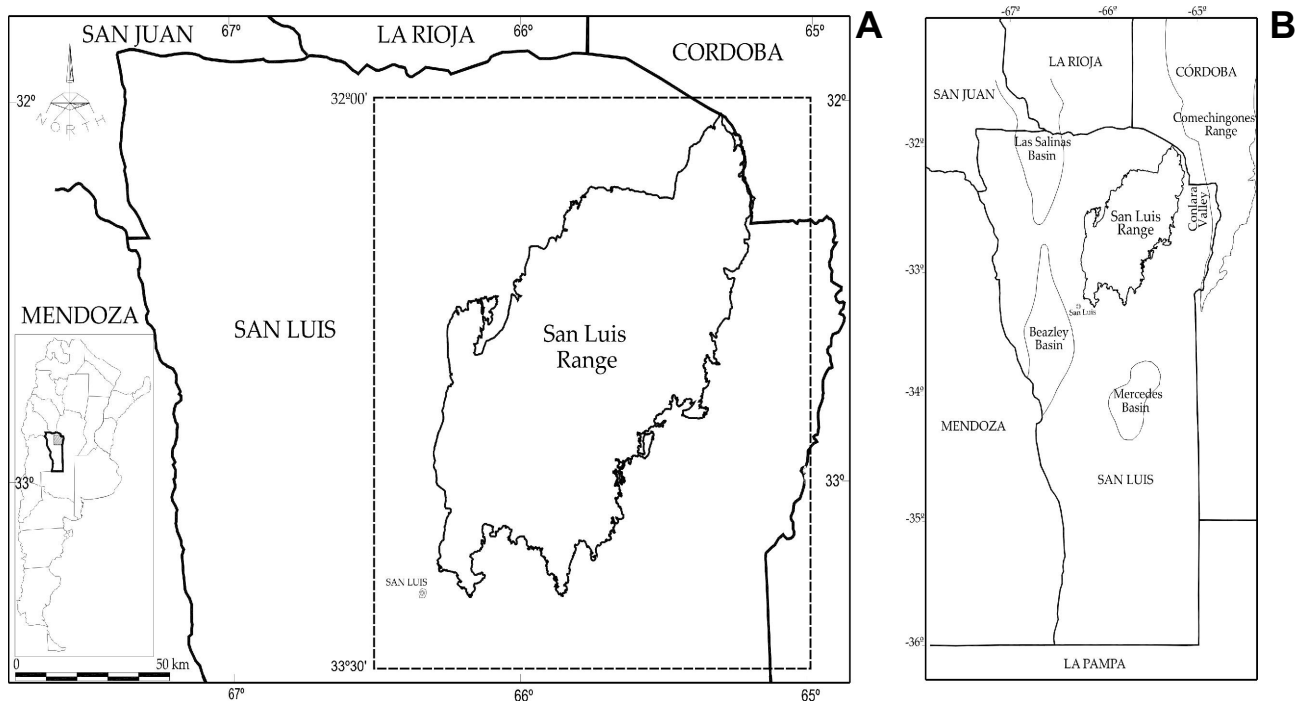


Figure 1. A: Geographic location of the San Luis range. **B:** Location of the sedimentary basins nearby the San Luis range (Modified from Criado-Roqué et al. 1981).

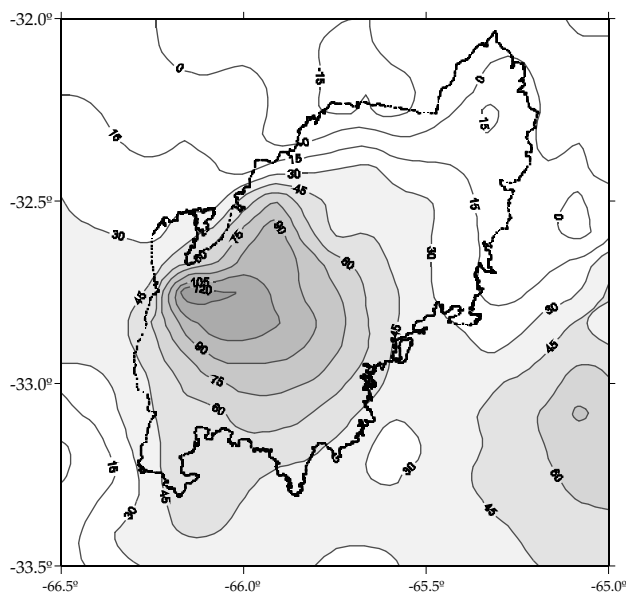


Figure 2. Observed free-air anomalies chart. Equidistance 15 mGal.

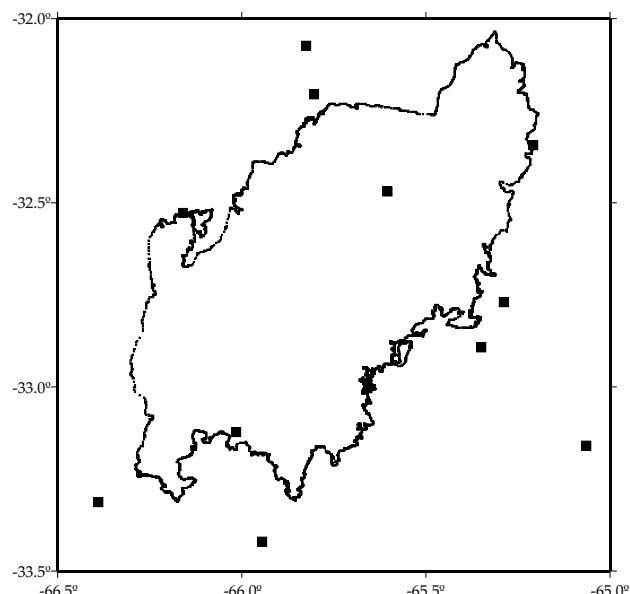


Figure 3. Geographic location of the geoid height stations $N = h - H$ of the San Luis Provincial Geodetic Network. Values $N = h - H$ were used as the control of N_f obtained in this work.

San Luis range basement is igneous-metamorphic. The main phase of the Famatinian orogenic cycle was responsible for delineating the most important features of the San Luis range basement. The Famatinian magmatic arc was active since Mid-Cambrian times (513 – 501 Ma) and the Ordovician was the climax of the magmatism, tectonism and metamorphism. From the regional point of view, the Ordovician deformation in Pampeanas Ranges was associated with terrane collision. The San Luis range is located at the proto-Andean margin on the Gondwana autochthon where the magmatic arc was emplaced.

DATA BASE

In this work we use gravity data and levelling heights. Both of them were obtained from IFIR (Instituto de Física Rosario) and IGM (Instituto Geográfico Militar) data bases. IFIR gravity measurements before 1997 have standard deviations of ± 0.3 mGal (Introcaso et al. 1992); 1997 IGM and IFIR gravity measurements present standard deviations of ± 0.1 mGal (Geophysics Group, IFIR). Values from Argentine Gravity Chart (Guspí et al. 1995) were incorporated to the calculations in order to avoid Gibbs phenomena.

Using the whole gravity values, free-air anomalies were calculated in IGSN 1971 system. On the other hand, long wavelength free-air anomalies obtained from both global geopotential EGM96 (Lemoine et al. 1998) and EIGEN GL03C (Förste et al. 2005) models were used in our calculations. Altimetry used here involves: (a) bench marks heights from IGM, (b) heights obtained from different gravity profiles on the San Luis range from IFIR data base, and (c), heights from digital elevation model (Gtopo30, U.S. Geological Survey EROS Data Center (EDC), 1996). Precision orders of these altitudes are: in (a), $\pm 3\text{mm}(L[\text{km}])^{1/2}$ and

$\pm 5\text{mm}(L[\text{km}])^{1/2}$ for high precision lines and precision lines respectively; $\pm 10\text{cm}(L[\text{km}])^{1/2}$ for topographic lines with L : length measured line in km; in (b), $\pm 1.00\text{m}$ (Geophysics Group, IFIR) and in (c) by comparing 269 heights on bench marks (high precision line and precision line) and altitudes in the same stations from the digital elevation model, we have obtained a relative porcentual error of 5 % (Cornaglia 2005). If we translate these values to gravity calculations, the maximum error on the observed anomalies is: (a) $\pm 0.03\text{mGal}$; (b) $\pm 0.30\text{mGal}$ and (c), $\pm 3.06\text{mGal}$ (only fitted values). These probability errors are adequated for our aims. So, different weights were assumed for building regular grids of observed free-air gravity anomalies.

We consider all values used here consistent enough to obtain a geoid undulations N chart to study the isostatic state of the San Luis range according to our purposes.

Gravity anomaly. Observed gravity values g_{obs} used here were connected to the fundamental Miguelete station of Buenos Aires (Argentina): 979690.03 mGal corresponding to IGSN71 [International Gravity Standarization Network 1971]. Then, we have used the traditional expression:

$$AAL = g_{\text{obs}} - (- c_{\text{AL}}) \quad (\text{Eq. 1})$$

where AAL is the free-air gravity anomaly (in mGal) (Fig. 2), is the normal gravity calculated with WGS84 ellipsoid and c_{AL} is the free-air correction, with $c_{\text{AL}} = 0.3086 H$ [mGal/m], being H : the altitude of the station. These free-air anomalies were assumed as Faye anomalies because, in view of the maturity of the relief, the terrain corrections are less than 4% (Cornaglia 2005). From Eq. 1 is possible to separate both free-air long wavelength and short wavelength anomalies.

Table 1. Amount of stations according to $E = N_T - N_C$ for different truncated spherical harmonic expansions. Proportionality factor $k = 1.4$ was assumed to define equivalent sources depth. In column (1) $E = N_T - N_C$ intervals assumed, with N_T : total geoid undulations obtained from Eq. 3, N_C : geoid undulations from the geometric definition $N_C = h - H$ (order precision approx. ± 0.05 m, see Figure 3) and E : residual difference; in column (2), the amount of stations for intervals E vs N_{LWL} from the EIGEN CG03C spherical harmonic expansion model truncated at $n = m = 36, 40, 50$ and 70 respectively, and on third column (3), EGM96 model results. Shaded cells point out that the largest amount of stations for the smallest E interval belongs to EIGEN CG03C model.

PROPORTIONALITY FACTOR 1.4								
Degree and order truncation								
(1)	(2)				(3)			
$N_T - N_C = E$ Intervals [m]	EIGEN CG03C				EGM96			
	36	40	50	70	36	40	50	70
0.00-0.25	5	8	4	5	6	5	4	5
0.25-0.50	4	2	5	4	2	5	5	4
0.50 -0.75	1	1	1	1	2	0	1	1
0.75 -1.00	1	0	1	1	1	1	1	1

Amount of
Stations

Table 2. Amount of stations according to $E = N_T - N_C$ for different truncated spherical harmonic expansions. Proportionality factor $k = 2.1$ was assumed to define equivalent sources depth. Columns (1) - (3) as in Table 1.

PROPORTIONALITY FACTOR 2.1								
Degree and order truncation								
(1)	(2)				(3)			
$N_T - N_C = E$ Intervals [m]	EIGEN CG03C				EGM96			
	36	40	50	70	36	40	50	70
0.00-0.25	5	8	4	5	5	5	5	6
0.25-0.50	4	2	5	4	3	5	3	3
0.50 -0.75	1	1	1	1	2	1	2	1
0.75 -1.00	1	0	1	1	1	0	1	1

Amount of
Stations

Table 3. Amount of stations according to $E = N_T - N_C$ for different truncated spherical harmonic expansions. Proportionality factor $k = 2.8$ was assumed to define equivalent sources depth. Columns (1) - (3) as in Table 1.

PROPORTIONALITY FACTOR 2.8								
Degree and order truncation								
(1)	(2)				(3)			
$N_T - N_C = E$ Intervals [m]	EIGEN CG03C				EGM96			
	36	40	50	70	36	40	50	70
0.00-0.25	6	6	4	6	4	4	5	6
0.25-0.50	2	4	5	1	4	5	3	3
0.50 -0.75	3	1	2	3	2	2	2	1
0.75 -1.00	0	0	0	1	1	0	1	1

Amount of
Stations

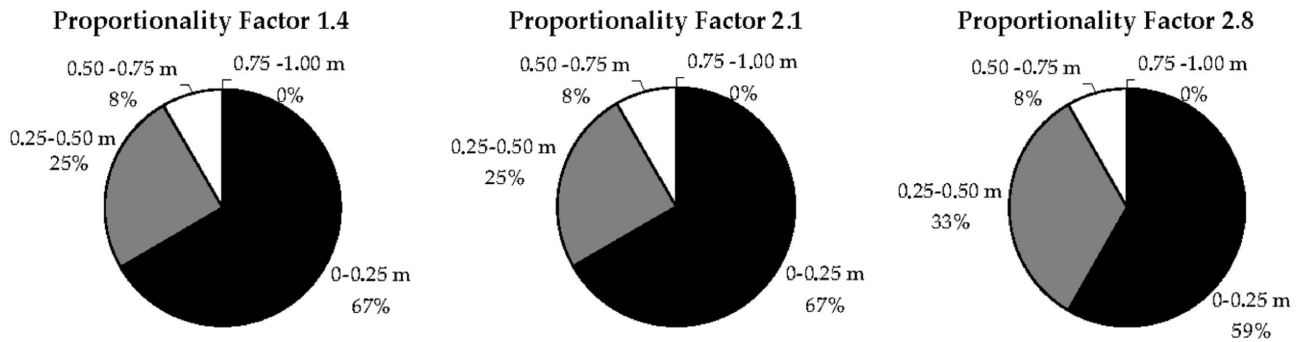
DEGREE AND ORDER OF TRUNCATION $n = m = 40$ 

Figure 4. Percentage of amount of stations in order to $E = N_T - N_C$ differences corresponding to $n = m = 40$ EIGEN CG03C in relation to the different proportionality factors used in calculation.

GEOID UNDULATIONS CHART OF THE SAN LUIS RANGE

Although the well known ambiguity of potential field is a serious problem to obtain a consistent gravity model by inversion, it can be put into advantage to calculate geoid undulations (Introcaso 2004, 2006). From the equivalent sources method (fictitious, simple, rigorous), it is possible to define a model (ensemble of sources) that fits observed free-air anomalies removed from long wavelength effects. Then, from this fictitious model, we can directly calculate the disturbing potential (or anomalous potential) T , then obtain N from the formula of Bruns: $N = T/g$ (see Torge 2001) with $g = 9.80 \text{ m/s}^2$ (Guspi et al. 2004, Introcaso & Crovetto 2005, Introcaso

2006). We have followed Guspi et al. (2004) who solved a linear equations system:

$$N_i = \frac{1}{\gamma} \sum_{j=1}^n T_{ji} = \frac{1}{\gamma} G \sum_{j=1}^n \frac{c_{ji}}{l_{ji}} \quad (\text{Eq. 2})$$

for obtaining the intensities of equivalent sources c_j . G is the gravitational constant $6.67 \times 10^{-8} \text{ cm}^3 \text{ g}^{-1} \text{ s}^{-2}$, T_{ji} is the disturbing potential at i station and l_{ji} is the distance from the station i to the source c_j . In order to calculate different long wavelength geoid undulations, the following expression was assumed:

$$N_T = N_{LWL} + N_{SWL} \quad (\text{Eq. 3})$$

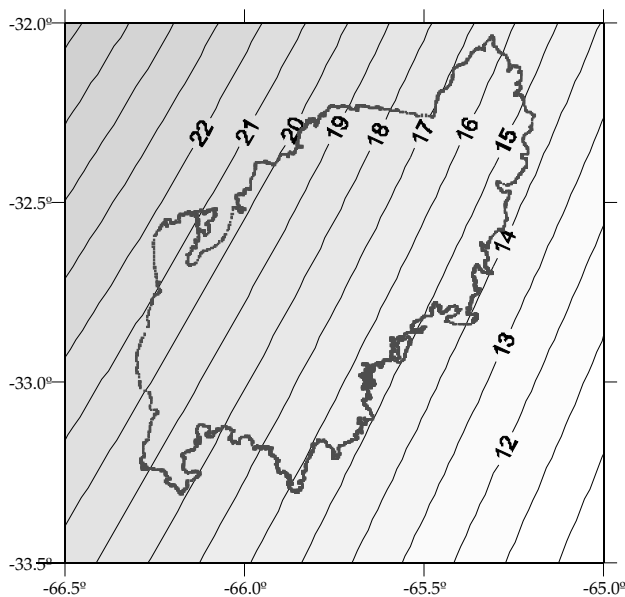


Figure 5. Free-air gravity anomalies AAL_{LWL} chart from EIGEN CG03C model developed up to $n = m = 40$. Contours each 1 mGal.

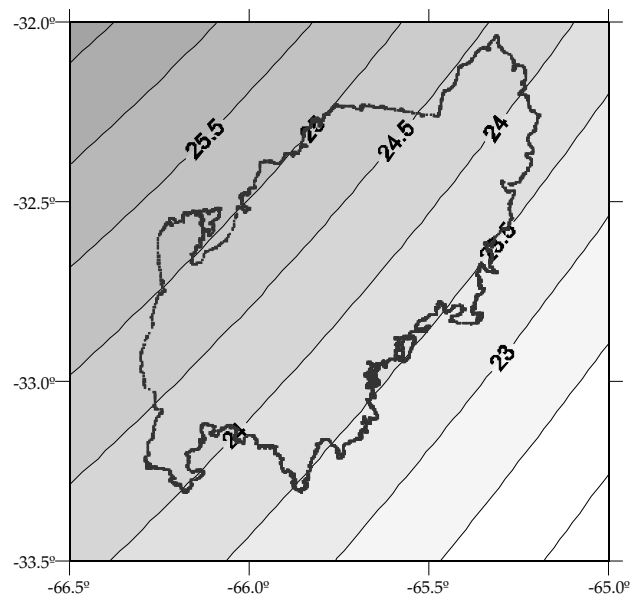


Figure 6. Geoid undulations N_{LWL} chart from EIGEN CG03C model developed up to $n = m = 40$. Contours each 0.25 m.

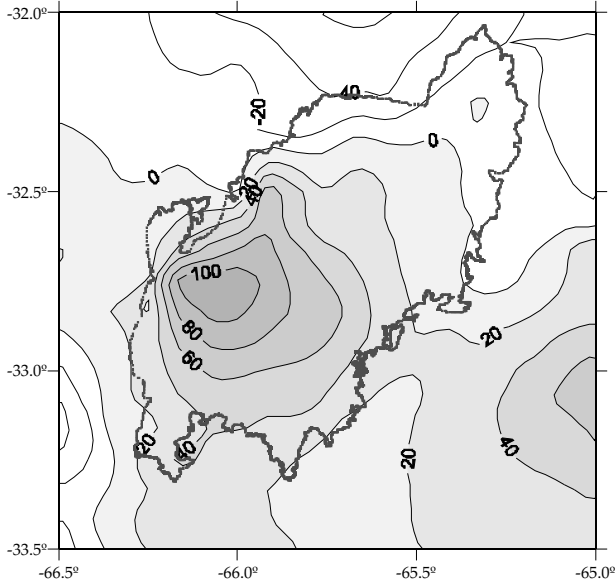


Figure 7. Short wavelength free-air anomalies chart obtained from Eq. 4. Contours each 15 mGal.

with N_T : total geoid undulations; N_{LWL} : long wavelength geoid undulations, and N_{SWL} : short wavelength geoid undulations. Very short wavelength geoid undulations are not necessary for our geophysical purposes. Geoid undulations N_T calculated here must not be confused with N geoid undulations given by global geopotential models (EIGEN or EGM) with lower resolution power. An expression similar to Eq. 3 was used for free-air anomalies:

$$AAL = AAL_{LWL} + AAL_{SWL} \quad (\text{Eq. 4})$$

with AAL : total observed free-air anomaly, AAL_{LWL} : long wavelength free-air anomaly, and AAL_{SWL} : short wavelength free-air anomaly. It is well known that in Eq. 3 and Eq. 4, N_{LWL} and AAL_{LWL} are very well defined from global geopotential models (Torge 2001, Introcaso 2006, among others). For calculation of N_{LWL} , we have started from a spherical harmonic expansion of N obtained using both global geopotential models EGM96 and EIGEN CG03C, involving the scale factor $N_0 = -53$ cm (Lemoine et al. 1998). Both global geopotential models (EGM96 and EIGEN CG03C) are practically identical. Then, we have truncated this spherical harmonic expansion at the following low-degrees: 36, 40, 50 and 70.

Several authors (Doin et al. 1996, Mc Kenzie et al. 1980, Sandwell & Renkin 1988, among others.), have just filtered the spherical harmonic expansion in different empirical low-degrees. In order to calculate N_{SWL} we have used short wavelength free-air anomalies. They were obtained from Eq. 4 with:

$$AAL_{SWL} = AAL - AAL_{LWL} \quad (\text{Eq. 5})$$

Then, with this gravity anomaly and the equivalent sources method the N_{SWL} chart was defined (Fig. 8); Fig. 5 shows AAL_{LWL} EIGEN CG03C cut in $n = m = 40$ (the step

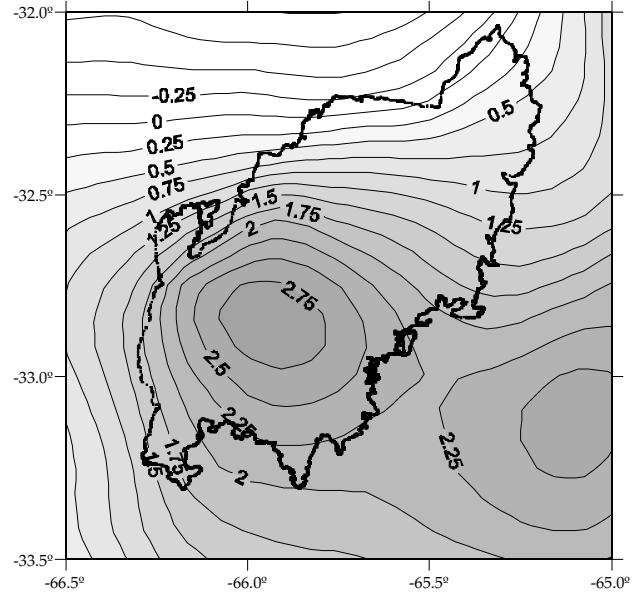


Figure 8. Short wavelength geoid undulations chart calculated from values in Fig. 7 and equivalent sources method. Contours each 0.25 mGal.

is 1 mGal); Fig. 6 shows N_{LWL} chart from EIGEN CG03C model cut in $n = m = 40$ (the step is 0.25 m); Fig. 7 shows AAL_{SWL} chart (the step is 15 mGal). Proportionality numbers for source depths were assumed following the criterion of Dampney (1969). Varying these numbers we have obtained the results shown in Tables 1-3. Each of them was combined with the spherical harmonic expansion geopotential model truncated at degree and order $n = m = 36, 40, 50$ and 70 for calculation of N_{LWL} . Tables 1-3 show: on the first column $(N_T - N_C) = E$ intervals: $[0-0.25]$ m; $[0.25-0.50]$ m; $[0.50-0.75]$ m and $[0.75-1.00]$ m assumed, with N_T : total geoid undulations obtained from Eq. 3, N_C : geoid undulations from the geometric definition $N_C = h - H$ (order precision approx. ± 0.05 m, Fig. 3) and E : residual difference; on the second column the amount of stations for intervals E versus N_{LWL} from the EIGEN CG03C spherical harmonic expansion model truncated at $n = m = 36, 40, 50$ and 70 respectively, and on third column, EGM96 model results.

Tables 1-3 correspond to proportionality factors: 1.4, 2.1 and 2.8 respectively. We have chosen N_{LWL} at $n = m = 40$ from EIGEN CG03C. Fig. 4 shows that results are practically the same thus we have decided to use $k = 1.4$ following Cordell (1992). Fig. 8 shows the geoid undulations chart corresponding to short wavelengths. It was obtained using free air anomalies (Fig. 7) and the equivalent sources method (step: 0.25 m). Fig. 9 shows the chart of total geoid undulations N_T obtained by adding short wavelength undulations values (Fig. 8) and values obtained using EIGEN CG03C model (Fig. 6) adjusted with eleven $N_C = h - H$ values (step: 0.25 m). The chart of geoid undulations obtained from the global geopotential model EIGEN CG03C is shown in Fig. 10. After comparison of the total geoid undulations chart obtained herein with geoid undulations chart in Fig. 10 (step: 0.25 m) we have found that this later has very poor resolution and different morphology.

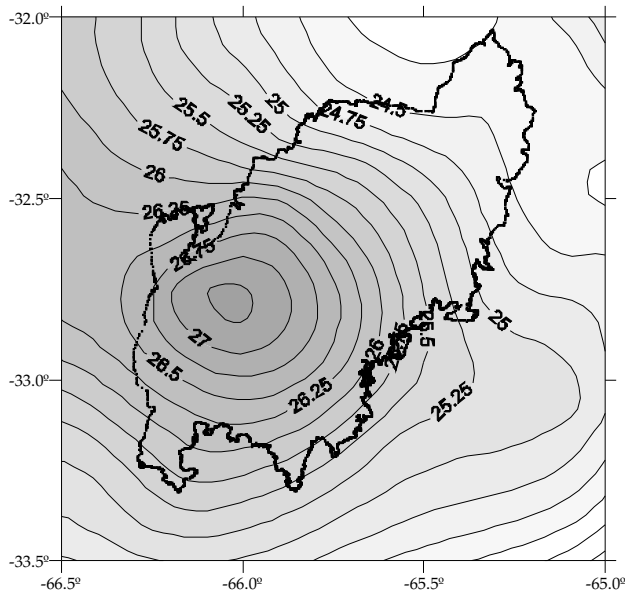


Figure 9. Chart of total geoid undulations N_T of the San Luis range obtained from Fig. 6 chart added to Fig. 8 chart using control stations $N_c = h - H$ in Fig. 3. Contours each 0.25 mGal.

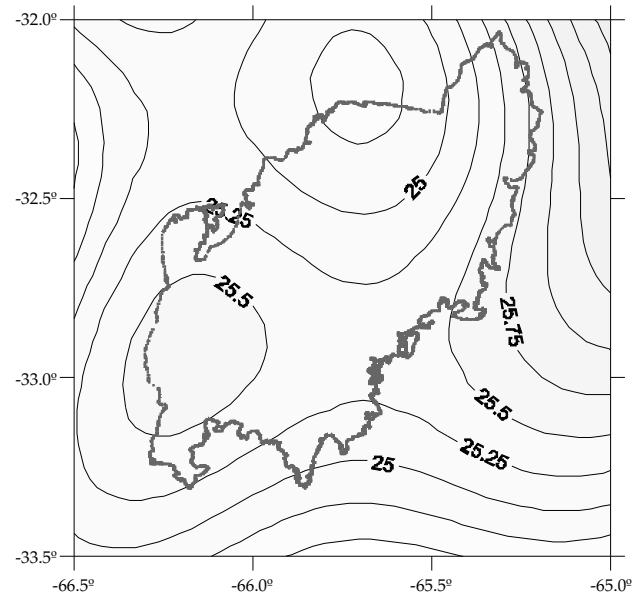


Figure 10. Total geoid undulations chart on the San Luis range obtained from the global geopotential model EIGEN CG03C. Contours each 0.25 mGal.

THEORETICAL COMPARISON MODEL

Ramé & Introcaso (1997) suggested that the San Luis range is apparently compensated in Airy system. In order to analyze the isostatic balance in Airy hypothesis we have prepared an isostatically compensated structural model for the San Luis range, starting with topography as tectonic input signal (Isacks 1988). We have assumed: a crustal thickness $T_N = 33$ km (Bullen 1963, Woollard 1969, Introcaso et al. 1992); R (crustal root) = $6.675 H_T$ with H_T : topographic altitude obtained from altimetry detailed in the data base. This isostatically balanced model (see Fig. 11) was obtained with $H_T + T_N + 6.675 H_T = T_N + 7.675 H_T$. In order to calculate the free-air anomalies we have assimilated the topography (Fig. 12) and the corresponding crustal roots as right and homogeneous parallelepipeds. The following equation (Okabe 1979) was employed:

$$g_z(x, y, z) = G\sigma' \left[x \ln(y+r) + y \ln(x+r) + \right. \\ \left. + 2z \arctan \frac{x+y+r}{z} \right] \bigg|_{\Delta x_1}^{\Delta x_2} \bigg|_{\Delta y_1}^{\Delta y_2} \bigg|_{\Delta z_1}^{\Delta z_2} \quad (\text{Eq. 6})$$

being g_z : gravity anomaly (positive effect for H_T and negative effect for R) on stations $E(x, y, z)$. x_i, y_i, z_i : distances between E and the vertices x_1, x_2, y_1, y_2 and z_1, z_2 of parallelepiped i , with $r = [(x_i)^2 + (y_i)^2 + (z_i)^2]^{1/2}$; G : gravitational constant ($6.67 \times 10^{-8} \text{ cm}^3 \text{ g}^{-1} \text{ s}^{-2}$) and σ' : density of the parallelepiped. Theoretical free-air anomalies were obtained from

$$AAL_{(\text{Theoretical})} = g_{z(\text{Topography})} + g_{z(\text{Crustal root})} \quad (\text{Eq. 7})$$

Fig. 13 exhibits free-air theoretical anomalies obtained from Eq. 7. There are different methods which can be employed for calculation of the disturbing isostatic potential T from free-air anomalies. For example: Stokes (in Torge 2001, among others), equivalent sources method, or the direct calculation of T (and N) from topography and crustal roots. We have used the equivalent sources method in order to show its versatility. Total geoid undulations involving isostatic effects were calculated using:

$$N_{iT} = N_{LWL} + N_{iLWL} \quad (\text{Eq. 8})$$

with N_{iT} : total isostatic geoid undulations (Fig. 14) involving N_{iLWL} : local isostatic geoid undulations obtained from theoretical free-air anomalies (Fig. 13) and N_{LWL} : long wavelength geoid undulations (Fig. 6).

Fig. 14 exhibits the total isostatic geoid undulations chart. Fig. 15A shows the location of profile AA' crossing NW-SE the San Luis range and Fig. 15B shows both results on AA' profile: real geoid undulations N_T and geoid undulations involving isostatic balance in Airy hypothesis N_{iT} which are in good agreement.

CONCLUSIONS

Two geoid undulations charts, N_T and N_{iT} , for the San Luis range were built. Both of them involve long wavelength geoid undulations N_{LWL} obtained by limiting the spherical harmonic expansion to degree and order 40 in the global geopotential model EIGEN CG03C. From observed residual free-air gravity anomalies and using the equivalent sources method we have obtained the geoid undulations chart N_{SWL} that was added to N_{LWL} for defining N_T . The second chart N_{iT} was built from local

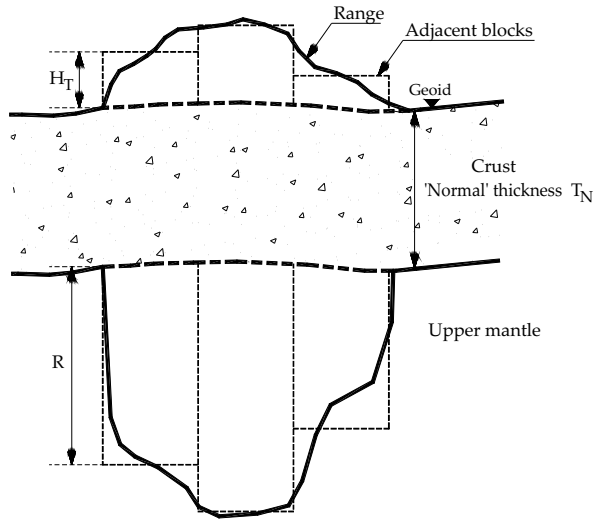


Figure 11. Schematic representation of the Airy isostatic system assumed for the San Luis range.

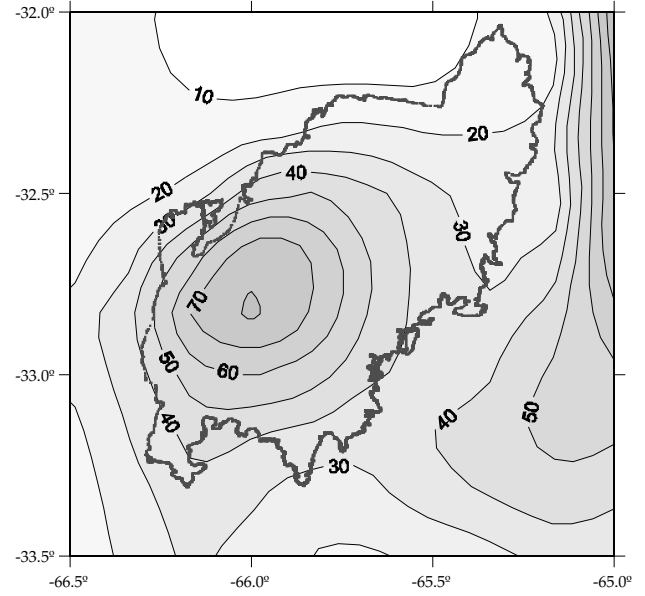


Figure 13. Theoretical free-air gravity anomalies chart (calculated from Eq. 7). Contours each 10 mGal.

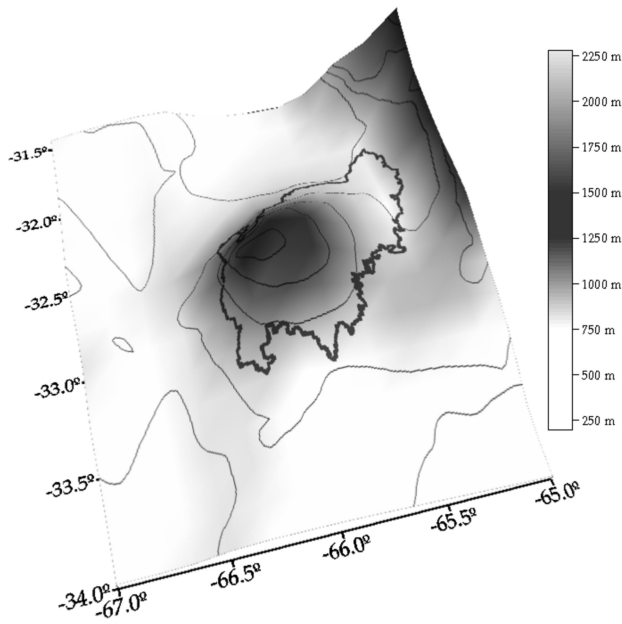


Figure 12. Smoothed topography of the San Luis range and surrounding area. Contours each 250 m.

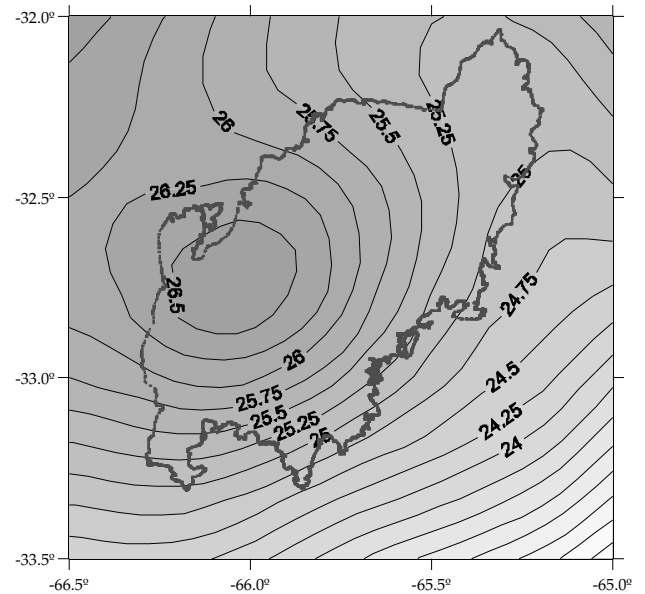


Figure 14. Geoid undulation chart that involves a perfect isostatic balance on the San Luis range. Contours each 0.5 m.

isostatic geoid undulations N_{iLWL} (short wavelength) obtained from crustal theoretical model in Airy isostatic equilibrium. Thus, $N_{iT} = N_{LWL} + N_{iLWL}$. By comparing both N_T and N_{iT} charts and a cross section on the range, we conclude that exists a good consistency between N_T and N_{iT} . Thus, there is a reasonable isostatic balance in Airy hypothesis. We show an alternative method for the analysis of the structural characteristics of the crust.

Acknowledgments

To Gustavo Ramé and Mario Giménez. This work was carried out during the Internal Postdoctoral Scholarship (CONICET) of L.L. Cornaglia. This study has partially been supported by the Agencia Nacional de Promoción Científica y Tecnológica (National Agency of Scientific and Technology Promotion) (PICTR 2002-00166). Graciela Font and an anonymous reviewer contributed for enhancing the manuscript as reviewers of the journal.

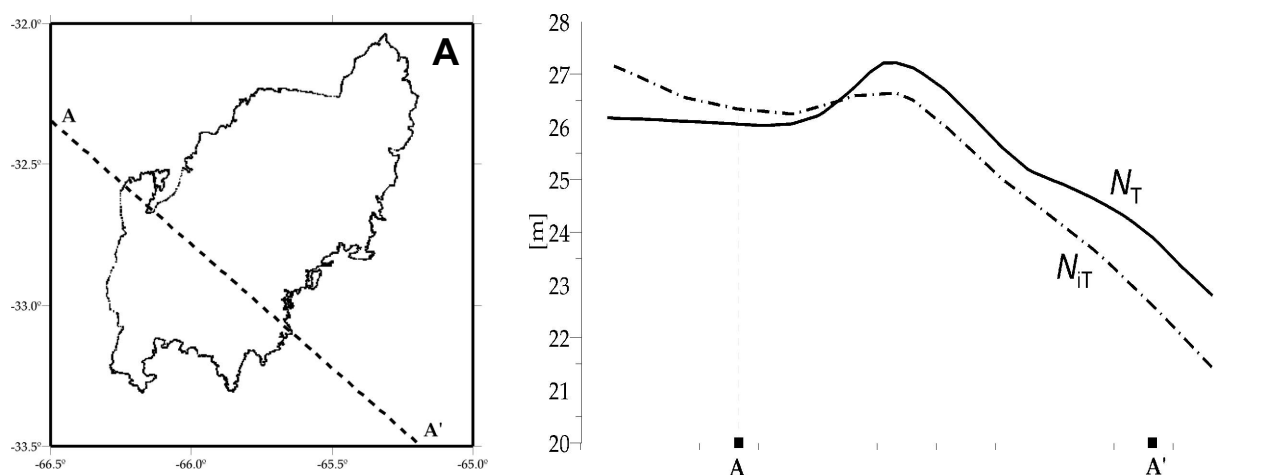


Figure 15. A: Geographic location of the cross section AA' used to compare in 2D geoid undulations from Figs. 9 and 14. B: 2D geoid undulations (N_T and N_{IT}) from Figs. 9 and 14 by comparing N_T built from data and N_{IT} from isostatically compensated model in Fig. 11, showing good agreement

REFERENCES

- Bullen K., 1963. An introduction to the theory of Seismology. Cambridge University Press, Cambridge. 381 p.
- Cornaglia L.L., 2005. Determinación del estado isostático y las características corticales de las Sierras de San Luis a partir de las ondulaciones del geoide. Tesis doctoral, Universidad Nacional de Rosario. 133 p. [Unpublished].
- Cornaglia L. & Introcaso A., 2004. Exceso de gravedad en al Sierra Grande de San Luis obtenido a partir de ondulaciones del geoide. Estudio preliminar realizado sobre una sección transversal (centrada en 32°50' S). *Geoacta* **29**: 1-9.
- Cordell, L. 1992. A scattered equivalent-source method for interpolation and gridding of potencial-field data in three dimensions. *Geophysics* **57**(4): 629-636.
- Criado-Roqué P., Mombrú C. & Ramos V., 1981. Estructura e interpretación tectónica. In: Yrigoyen, M. (Ed.). *Geología de la Provincia de San Luis. Relatorio del Octavo Congreso Geológico Argentino*: 155-192.
- Crovetto C. & Introcaso A., 2004. Indicadores isostáticos geoidicos. Un ejemplo para la sierra de San Luis. *Geoacta* **29**: 49-56.
- Dampney C.N.G., 1969. The equivalent source technique. *Geophysics* **34**(1): 39-53.
- Doin M.P., Fleitout L. & McKenzie D., 1996. Geoid anomalies and the structure of continental and oceanic lithospheres. *Journal of Geophysical Research* **101**(B7): 16119-16135.
- Förste C., Flechtner F., Schmidt R., Meyer U., Stubenvoll R., Barthelmes F., König R., Neumayer K.H., Rothacher M., Reigber C., Biancale R., Bruinsma S., Lemoine J.-M. & Raimondo J.C., 2005. A New High Resolution Global Gravity Field Model Derived From Combination of GRACE and CHAMP Mission and Altimetry/Gravimetry Surface Gravity Data. *Poster presented at EGU General Assembly 2005 (April), Vienna, 24-29*.
- Guspí F., Introcaso A. & Pacino M.C., 1995. Carta gravimétrica argentina 1995: su construcción. *Actas Congreso Argentino de Geociencias y Geotectónicas & Noveno Congreso Nacional de Cartografía*, Buenos Aires, Centro Argentino de Cartografía **1**: 88-93.
- Guspí F., Introcaso A. & Introcaso B., 2004. Gravity-enhanced representation of measured geoid undulations using equivalent sources. *Geophysical Journal International (RAS)* **158**: 1-8.
- Introcaso A., 2004. Ambigüedad en la inversión del campo potencial. Sus ventajas para la obtención del geoide local. *Tópicos de Geociencias* (Editorial Fundación Universidad Nacional de San Juan): 255-267.
- Introcaso A., 2006. Geodesia Física. *Boletín del Instituto de Fisiografía y Geología Vol. Especial 1*: 1-128.
- Introcaso A., Pacino M.C. & Fraga H., 1992. Gravity, isostasy and Andean crustal shortening between latitudes 30°S and 35°S. *Tectonophysics* **205**: 31-48.
- Introcaso A. & Crovetto C., 2005. Introducción a la construcción del geoide. *Temas de geociencia* **12**: 1-56.
- Isacks B., 1988. Uplift of the central Andean Plateau and bending of the Bolivian Orocline. *Journal of Geophysical Research* **93**(B4): 3211-3231.
- Jordan T.E. & Allmendinger R.W., 1986. The Sierras Pampeanas of Argentina: A modern analogue of rocky mountain foreland deformation. *American Journal of Science* **286**: 737-764.
- Lemoine F., Kenyon S., Factor J., Trimmer R., Pavlis N., Chiuw D., Cox C., Klosko S., Luthcke S., Torrence M., Wang Y., Williamson R., Pavlis H., Rapp R. & Olson T., 1998. The development of the joint NASA, CSFC and NIMA geopotential model EGM96, NASA/TP, 1998 – 206861, Goddard Space Flight Center.
- McKenzie D., Watts A., Pearson B. & Roufosse M., 1980. Platform and mantle convection beneath the Pacific Ocean. *Nature* **288**: 442-446.
- Okabe M., 1979. Analytical expressions for gravity anomalies due to homogeneous polyhedral bodies and translations into magnetic anomalies. *Geophysics* **44**(4): 730-741.
- Ramé G. & Introcaso A., 1997. Análisis isostático

- preliminar de la Sierra Grande de San Luis, Argentina. *Revista de la Asociación Geológica Argentina* **53(3)**: 379-386.
- Sandwell D. & Renkin M.L., 1988. Compensation of swells and plateaus in the North Pacific. *Journal of Geophysical Research* **93(B4)**: 2775-2783.
- Sato A.M., Gonzalez P.D. & Llambías E.J., 2003. Evolución del orógeno Famatiniano en la Sierra de San Luis: magmatismo de arco, deformación y metamorfismo de bajo a alto grado. *Revista de la Asociación Geológica Argentina* **58(4)**: 487-504.
- Torge W., 2001. Geodesy (3rd edition). *Walter de Gruyter*. Berlin-New York. 416 p.
- Woollard G., 1969. Regional Variations in Gravity. Geophysical Monograph. *American Geophysical Union* **13**: 320-341.